Applied and Environmental Microbiology, Sept. 2010, p. 6239–6247 Vol. 76, No. 18
0099-2240/10/$12.00 doi:10.1128/AEM.01104-10

Combined Gel Probe and Isotope Labeling Technique for Measuring Dissimilatory Nitrate Reduction to Ammonium in Sediments at Millimeter-Level Resolution[▽]

Peter Stief,* Anna Behrendt, Gaute Lavik, and Dirk De Beer

Max Planck Institute for Marine Microbiology, Celsiusstraße 1, 28359 Bremen, Germany

Received 7 May 2010/Accepted 13 July 2010

Dissimilatory NO_3^- reduction in sediments is often measured in bulk incubations that destroy *in situ* gradients of controlling factors such as sulfide and oxygen. Additionally, the use of unnaturally high NO_3^- concentrations yields potential rather than actual activities of dissimilatory NO_3^- reduction. We developed a technique to determine the vertical distribution of the net rates of dissimilatory nitrate reduction to ammonium (DNRA) with minimal physical disturbance in intact sediment cores at millimeter-level resolution. This allows DNRA activity to be directly linked to the microenvironmental conditions in the layer of NO_3^- consumption. The water column of the sediment core is amended with $^{15}NO_3^-$ at the *in situ* $^{14}NO_3^-$ concentration. A gel probe is deployed in the sediment and is retrieved after complete diffusive equilibration between the gel and the sediment pore water. The gel is then sliced and the NH_4^+ dissolved in the gel slices is chemically converted by hypobromite to N_2 in reaction vials. The isotopic composition of N_2 is determined by mass spectrometry. We used the combined gel probe and isotopic labeling technique with freshwater and marine sediment cores and with sterile quartz sand with artificial gradients of $^{15}NH_4^+$. The results were compared to the NH_4^+ microsensor profiles measured in freshwater sediment and quartz sand and to the N_2O microsensor profiles measured in acetylene-amended sediments to trace denitrification.

Nitrate accounts for the eutrophication of many human-affected aquatic ecosystems (19, 21). Sediment bacteria may mitigate NO_3^- pollution by denitrification and anaerobic ammonium oxidation (anammox), which produce N_2 (13, 18). However, inorganic nitrogen is retained in aquatic ecosystems when sediment bacteria reduce NO_3^- to NH_4^+ by dissimilatory nitrate reduction to ammonium (DNRA) (5, 12, 16, 39). Hence, DNRA contributes to rather than counteracts eutrophication (23). DNRA may be the dominant pathway of dissimilatory NO_3^- reduction in sediments that are rich in electron donors, such as labile organic carbon and sulfide (4, 8, 17, 38, 55). High rates of DNRA are thus found in sediments affected by coastal aquaculture (8, 36) and settling algal blooms (16).

DNRA, denitrification, and the chemical factors that control the partitioning between them (e.g., sulfide) should ideally be investigated in undisturbed sediments. The redox stratification of sediments involves vertical concentration gradients of pore water solutes. These gradients are often very steep, and their measurement requires high-resolution techniques, such as microsensors (26, 42) and gel probes (9, 54). If, for instance, the influence of sulfide on DNRA and denitrification is to be investigated, one wants to know exactly the sulfide concentration in the layers of DNRA and denitrification activity, as well as the flux of sulfide into these layers. This information can easily be obtained using H_2S and pH microsensors (22, 43). It is less trivial to determine the vertical distribution of DNRA and denitrification activity in undisturbed sediments. Denitrification activity can be traced using a combination of the acetylene inhibition technique (51) and N_2O microsensors (1). Acetylene inhibits the last step of denitrification, and therefore, N_2O accumulates in the layer of denitrification activity (44). This method underestimates the denitrification activity in sediments with high rates of coupled nitrification-denitrification because acetylene also inhibits nitrification (50).

The vertical distribution of DNRA activity in undisturbed sediment has, to the best of our knowledge, never been determined; thus, the microenvironmental conditions in the layer of DNRA activity remain unknown. Until now, the influence of chemical factors on DNRA and denitrification in sediments has been assessed by slurry incubations (4, 12, 30), by flux measurements with sealed sediment cores (7, 47) or flowthrough sediment cores (16, 27, 37), and in one case, in reconstituted sediment cores sliced at centimeter-level resolution (39). Here, we present a new method, the combined gel probe and isotope labeling technique, to determine the vertical distribution of the net rates of DNRA in sediments. The sediments remain largely undisturbed and the NO_3^- amendments are within the range of *in situ* concentrations. The DNRA measurements can be related to the microprofiles of potential influencing factors measured in close vicinity of the gel probe. This allows DNRA activity to be directly linked with the microenvironmental conditions in the sediment.

MATERIALS AND METHODS

Sediment incubations. Different types of sediment were collected and incubated in different types of containers. (i) Freshwater sediment was collected on the banks of the Weser River approximately 10 km upstream of Bremen (northern Germany) in September 2007. In the laboratory, the sediment was sieved through a 1-mm mesh to remove the macrofauna and then used to fill benthic

* Corresponding author. Mailing address: Microsensor Group, Max Planck Institute for Marine Microbiology, Celsiusstraße 1, 28359 Bremen, Germany. Phone: 49 421 2028838. Fax: 49 421 2028690. E-mail: pstief@mpi-bremen.de.

▽ Published ahead of print on 23 July 2010.

gradient chambers (BGCs) (40). In the BGC, the sediment is placed in a vertical tube (inner diameter = 4.5 cm, height = 4.5 cm) that is sandwiched between two water-filled reservoirs. The bottom side of the tube is closed with a 63-μm-pore-size plastic mesh. The top reservoir contained 1.5 liters aerated potable water in which the NO_3^- concentration was adjusted to 250 μmol liter^{-1}, which corresponded to the *in situ* concentration at the time of sampling. The bottom reservoir contained 3.7 liters of deoxygenated and autoclaved potable water in which the NH_4^+ concentration was adjusted to 500 μmol liter^{-1}. Initially, the potable water in the bottom reservoir contained 35 μmol liter^{-1} NO_3^-, which was completely consumed within less than 3 days and not replenished afterwards. Both reservoirs were static (i.e., there was no flowthrough), and therefore, the NO_3^- and NH_4^+ concentrations were repeatedly checked and readjusted to the wanted value, when indicated. The oxygen concentrations in the top and bottom reservoirs corresponded to 100 and 0% air saturation, respectively, throughout the incubation period and did not have to be readjusted. The BGCs were incubated at 21°C for 4 weeks, with all measurements being completed in weeks 3 and 4.

(ii) Marine sediment was collected with acrylic core liners (inner diameter = 9 cm, height = 20 cm) from an intertidal flat approximately 20 km north of Bremerhaven (Lower Saxony, Germany) in September 2009. This site is still in reach of the plume of the Weser River and shows pronounced annual fluctuations of the water column NO_3^- concentration of between 0 and ~100 μmol liter^{-1}. The intact sediment cores were incubated in the laboratory at 21°C for 2 weeks, during which all measurements were completed. The aerated seawater overlying the sediment was adjusted to contain NO_3^- at a concentration of 50 μmol liter^{-1} and was continuously replenished from a 10-liter reservoir at a high exchange rate to keep the NO_3^- concentration stable.

(iii) Quartz sand (type Geba; grain diameter = 0.06 to 0.3 mm; Carlo AG, Bern, Switzerland) was washed 3 times with deionized water, autoclaved, and dried. The washed quartz sand (400 ml each) was used to fill a modified BGC (inner diameter = 8 cm, height = 8 cm) with flowthrough top and bottom reservoirs (200 ml each). The top reservoir was continuously replenished with potable water that contained no NH_4^+, whereas the bottom reservoir was continuously replenished with potable water adjusted to contain $^{15}NH_4^+$ (99% ^{15}N atom %; Cambridge Isotope Laboratories, Andover, MA) at a concentration of 250 μmol liter^{-1}. The modified BGCs were incubated at 21°C for 2 weeks, with all measurements being completed in week 2.

Combined gel probe and isotope labeling technique. Polyacrylamide gel probes were constructed and assembled as described previously (25). The gels were cast from 40 ml acrylamide (15%, wt/vol), 20 ml *N*,*N*-methylenebisacrylamide (2%, wt/vol), 0.75 ml dipotassium peroxodisulfate (0.11 M), and 60 μl tetramethylethylenediamine. Dipotassium peroxodisulfate rather than ammonium peroxodisulfate was used to avoid interference by the excess NH_4^+ leaching from the gel (25). After hydration in deionized water (freshwater sediment, quartz sand) or in NaCl solution with a salinity of 25 (marine sediment), the gels were 2 mm thick. The hydrated gels were mounted onto homemade plastic probes with an aperture of 80 by 20 mm (see the schematic drawing in reference 25). The assembled probes were 120 mm long, 30 mm wide, and 4 mm thick (including the gel). This assembly was stored in deionized water or NaCl solution at 4°C until it was used for the experiments.

Forty-eight hours prior to deployment of the gel probes, the freshwater and marine sediments were overlain with ^{15}N-labeled NO_3^- (99% ^{15}N atom %; Cambridge Isotope Laboratories) at concentrations of 250 and 50 μmol liter^{-1}, respectively. The gel probes were deoxygenated with He, vertically inserted into the sediments, and allowed to equilibrate with the pore water for 24 h. The time needed for complete diffusive equilibration for the 2-mm-thick gel was <3 h (calculated from the data in reference 25), but a longer exposure time was scheduled to allow pore water gradients to reestablish after the physical disturbance due to insertion of the gel probe. After retrieval, the gels were quickly cut out of the aperture with a clean scalpel, blotted dry, and spread out evenly on a clean surface. In the experiments with freshwater sediment and quartz sand, the gels were sliced with an egg cutter, which resulted in a vertical resolution of 2.5 mm. In the experiment with marine sediment, a homemade cutter with blades of stainless steel was used, which resulted in a vertical resolution of 1.0 mm. The retrieval, cutting, and slicing of the gels and the distribution of the gel slices to preweighed 3-ml vials (Exetainer; Labco, High Wycombe, United Kingdom) were accomplished by two cooperating persons in 60 s. The vials were closed, weighed, and flushed twice with He for 30 s (with a 5-min equilibration time in between) to remove the N_2 from both the gel slices and the headspace of the vials. Two hundred microliters of 12 M NaOH was injected into the vials to convert NH_4^+ to NH_3, followed by the addition of 50 μl hypobromite to convert NH_3 to N_2 (56). The latter reaction was allowed to proceed for 3 days in the dark at 21°C. In headspace samples of 250 to 500 μl, the isotope ratio of $^{28}N_2$, $^{29}N_2$, and $^{30}N_2$ was determined by gas chromatography-isotopic ratio mass spectrometry (VG Optima; Isotech, Middlewich, United Kingdom) against air standards.

Calibration standards were prepared either in quartz sand that was thoroughly mixed with potable water or directly in potable water adjusted to contain $^{15}NH_4^+$ at different concentrations. Calibration series were prepared either in the low concentration range (0, 5, 10, and 25 μmol liter^{-1}) or in the high concentration range (0, 25, 50, and 100 μmol liter^{-1}). The gel probes were vertically inserted into the $^{15}NH_4^+$-spiked quartz sand or immersed in potable water and allowed to equilibrate for 24 h. After retrieval, the gels were treated in the same way as described above. For each $^{15}NH_4^+$ concentration, four to five replicate gel slices were analyzed. Calibration standards were generally prepared with the same batches of gels and hypobromite used for the samples, thereby avoiding inconsistencies due to different gel properties and efficiencies of the hypobromite assay in oxidizing $^{15}NH_4^+$ to N_2. The $^{15}NH_4^+$ concentration in the gel slices was calculated from the isotope ratio of $^{28}N_2$, $^{29}N_2$, and $^{30}N_2$ (35) and was corrected for the efficiency of the hypobromite assay with the calibration standards. The $^{15}NH_4^+$ concentration profiles in the sediment were assembled by calculating the vertical dimension of each gel slice from its wet weight and the known weight of a 1-cm gel slice. The vertical distribution of DNRA activity in the sediment was obtained by diffusion reaction modeling of the steady-state $^{15}NH_4^+$ concentration profiles (see below).

Additional testing of the new technique. In order to measure the DNRA activity in the sediment, any trace of ^{15}N-labeled N_2 due to denitrification activity must be removed from the gel slice before hypobromite is added to the reaction vial. This is achieved by repeated flushing of the reaction vial with He (see above). However, this may also lead to a loss of $^{15}NH_4^+$ in the form of gaseous $^{15}NH_3$. The effect of He flushing on the recovery of $^{15}NH_4^+$ was evaluated with additional calibration standards that were acidified with 50 μl of 1 N HCl to shift the NH_4^+-NH_3 equilibrium toward NH_4^+ to minimize the loss of gaseous NH_3. The following treatments were compared: (i) 2 min He flushing with no HCl, (ii) 20 min He flushing with no HCl, (iii) 2 min He flushing with 1 N HCl, and (iv) 20 min He flushing with 1 N HCl.

Conventional gel probe measurements. Currently, a microsensor for measurement of the NH_4^+ concentration in seawater is not available. Thus, pore water NH_4^+ concentrations were measured with gel probes, as described previously (34). Gel probes were deployed, retrieved, and sliced as described above. Ammonium was eluted from 50-μl gel slices in 1,100 μl deionized water for 30 min. The eluted NH_4^+ was photometrically quantified, as described previously (24). Calibration standards (0 to 250 μmol liter^{-1}) were prepared as described for $^{15}NH_4^+$ and processed in the same way as the samples. The measurement of the pore water NO_3^- concentration with gel probes as described previously (34) failed for unknown reasons.

Microsensor measurements and rate calculations. Microsensors for O_2 (41), H_2S (22), NO_3^-, NH_4^+, pH (cf. reference 11), and N_2O (1) were constructed in our laboratory. The LIX-type microsensors for NO_3^- and NH_4^+ mentioned here (cf. reference 11) can be used only in freshwater. The sensors were calibrated and used for profiling in a measuring setup, as described previously (52). The custom-made programs μ-Profiler, DAQ server, and LINPOS server were used for measurement automation and data acquisition (L. Polerecky, MPI Bremen; http://www.microsen-wiki.net). Vertical profiles were recorded at increments of 250 or 500 μm, starting in the overlying water and ending 10 to 35 mm below the sediment surface. Steady-state NO_3^-, NH_4^+, and N_2O concentration profiles were used to calculate net local conversion rates by diffusion reaction modeling, as detailed elsewhere (31). The sedimentary diffusion coefficients (D_s) of NO_3^-, NH_4^+, and N_2O were calculated from the respective diffusion coefficients in water (D_w) and the sediment porosity (Φ), as follows: $D_s = D_w \times \Phi/[1 - \ln(\Phi^2)]$ (2). The D_w values of NO_3^-, NH_4^+, and N_2O at 21°C were taken to be 1.72×10^{-5}, 1.78×10^{-5}, and 2.12×10^{-5} cm^2 s^{-1}, respectively (3, 29). Sediment porosity was measured as the loss of weight that occurred after a known volume of wet sediment was dried at 60°C for 48 h. The freshwater and marine sediments used in this study had porosities of 47 and 43%, respectively. Replicate concentration profiles were analyzed separately, the production-consumption profiles obtained were averaged, and the standard deviation of the mean rate was calculated for each depth layer.

The vertical distributions of DNRA and denitrification activity were derived from the concentration profiles of $^{15}NH_4^+$ (determined by the gel probe technique) and N_2O (determined with microsensors), respectively. For the latter, N_2O microprofiles were measured in separate sediment cores 16 h after inhibition of the last step of denitrification with acetylene (51). This method accounts for the denitrification activity driven by NO_3^- from the water column but not from sedimentary nitrification activity. The layers of DNRA and denitrification activity in the sediment (i.e., the layers of net $^{15}NH_4^+$ and N_2O production, respectively) were contrasted with the layers of net NO_3^- consumption and net

total NH_4^+ ($NH_4^+{}_{tot}$; i.e., $^{14}NH_4^+$ and $^{15}NH_4^+$) production in plots in which all other N conversions were omitted for clarity.

RESULTS

Calibration, precision, and optimization of the new technique. Figure 1 shows two representative examples of calibrations in quartz sand with pore water adjusted to low (Fig. 1A) and high (Fig. 1B) $^{15}NH_4^+$ concentration ranges. Calibrations were linear over the ranges 0 to 25 and 0 to 100 μmol liter^{-1} $^{15}NH_4^+$, with the R^2 values being 0.988 and 0.962, respectively. In the examples shown, the efficiency of the hypobromite assay at oxidizing NH_4^+ to N_2 was 96 to 98%. The lowest efficiency of the hypobromite assay encountered in this study was 60 to 74%. Calibrations in potable water were identical to those in quartz sand (data not shown).

Ten independent calibration series were analyzed to determine the absolute precision of the new technique (Table 1). Over the concentration range of from 0 to 25 μmol liter^{-1}, the standard deviation varied, on average, between 1.1 and 2.0 μmol liter^{-1} $^{15}NH_4^+$. At 50 and 100 μmol liter^{-1}, the average standard deviations were 3.7 and 11.1 μmol liter^{-1} $^{15}NH_4^+$, respectively. The latter two concentrations, however, were tested only a few times.

The effect of He flushing of acidified and nonacidified samples was evaluated in four independent calibration series (Table 2). The percent recovery of $^{15}NH_4^+$ was considerably higher in samples flushed with He 2 times for 1 min each time (2× 1 min) than for those flushed once for 20 min. Acidification of the samples with 1 N HCl increased the percent recovery of $^{15}NH_4^+$ and improved the linear fit of the calibration curves. The rate of $^{15}NH_4^+$ recovery from acidified samples flushed with He for 2× 1 min was slightly higher than 100%, which was due to the low absolute precision of the technique in the lower concentration range (Table 1).

Measurement of artificial $^{15}NH_4^+$ pore water gradients. $^{15}NH_4^+$ was the only form of NH_4^+ in quartz sand that was overlain with plain potable water and underlain with $^{15}NH_4^+$-amended potable water (Fig. 2). Thus, the vertical gradient of $^{15}NH_4^+$ could be equally measured by the combined gel probe and isotope labeling technique and by ion-selective microsensors. Both methods measured a close-to-linear concentration gradient of $^{15}NH_4^+$ in the quartz sand, and very good agreement between the gel probe and microsensor profiles was found. The average deviation between the two methods was 0.6 μmol liter^{-1} $^{15}NH_4^+$ or 1.6% for the full concentration range. The gel probe technique produced maximum deviations of −8.8 and +7.3 μmol liter^{-1} $^{15}NH_4^+$ from the microsensor data. The absolute precisions of gel probes and microsensors in the high concentration range (i.e., 100 to 145 μmol liter^{-1} $^{15}NH_4^+$) were, on average, 27 and 16 μmol liter^{-1}, respectively. The relative precisions of the gel probes and microsensors in this concentration range were, on average, 23 and 14%, respectively.

Concentration profiles in freshwater sediment. Stream sediment was sandwiched between aerated overlying water amended with $^{15}NO_3^-$ and anoxic underlying water amended with NH_4^+ in BGC. Figure 3 shows the average concentration profiles measured in three replicate BGCs; microsensor profiles were also repeated 2 to 4 times at random positions within

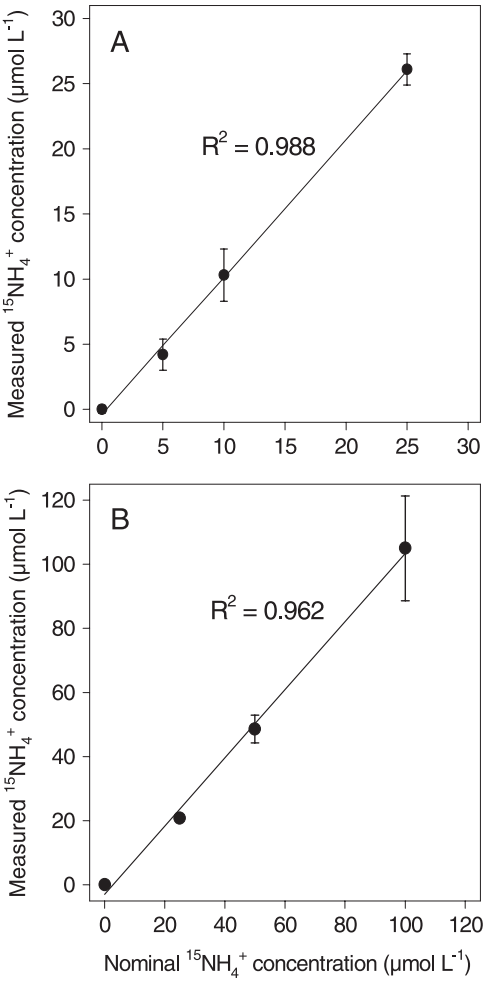

FIG. 1. Calibration of gel probes in the low (A) and high (B) range of $^{15}NH_4^+$ concentrations. Gel probes were incubated in potable water adjusted to contain $^{15}NH_4^+$ at known concentrations for 24 h. After retrieval, replicate gel slices were subjected to hypobromite oxidation for subsequent analysis of ^{15}N-labeled N_2 species. The means ± standard deviations of four to five replicates and the coefficients of determination for the regression line are shown.

each BGC. The vertical $^{15}NH_4^+$ profile showed a peak concentration of 14.3 μmol liter^{-1} at the 9.3-mm depth in the sediment of one of the three replicate BGCs (Fig. 3A). From the peak concentration, the $^{15}NH_4^+$ concentration decreased toward both the sediment surface and the deeper layers in the sediment, but no other conspicuous features in the profile were found. The average standard deviation for all depth intervals was 1.5 μmol liter^{-1} $^{15}NH_4^+$. The N_2O profiles measured in acetylene-inhibited stream sediment (incubated in a separate BGC) showed an average peak concentration of 91 μmol liter^{-1} at the 6-mm depth (Fig. 3B). The NO_3^- concentration decreased from 289 μmol liter^{-1} in the overlying water to 5 μmol liter^{-1} at the 10-mm depth and remained constant below that depth (Fig. 3C). The $NH_4^+{}_{tot}$ (i.e., $^{14}NH_4^+$ + $^{15}NH_4^+$) concentration (as measured with the LIX-type microsensor) increased from 1 μmol liter^{-1} in the overlying water to 191 μmol liter^{-1} at the 25-mm depth (Fig. 3C). At the 9.3-mm depth, where the maximum $^{15}NH_4^+$ concentration of 11 μmol

TABLE 1. Precision of combined gel probe and isotope labeling technique[a]

$^{15}NH_4^+$ concn (μmol liter^{-1})	Avg SD	No. of calibration series
0	1.1	10
5	1.5	7
10	2.0	9
25	1.8	9
50	3.7	3
100	11.1	2

[a] Ten independent calibration series with different concentration ranges were evaluated. The average standard deviations given here were calculated from 2 to 10 standard deviations of four to five replicates, each measured at the same $^{15}NH_4^+$ concentration.

liter^{-1} was measured with the gel probe, an $NH_4^+{}_{tot}$ concentration of 81 μmol liter^{-1} was measured with the microsensor. The O_2 concentration decreased from 278 μmol liter^{-1} in the overlying water to 0 μmol liter^{-1} at the 3-mm depth (Fig. 3D). The total sulfide concentration in the overlying water was near the detection limit of 1 μmol liter^{-1} of the H_2S microsensor and increased to 3.6 μmol liter^{-1} at the 25-mm depth (Fig. 3D). The pH value dropped from 8.0 in the overlying water to 6.8 at the 25-mm depth (Fig. 3D).

Local conversion rates of $^{15}NH_4^+$, N_2O, $NH_4^+{}_{tot}$, and NO_3^- in freshwater sediment. Net local conversion rates were calculated from the steady-state concentration profiles of $^{15}NH_4^+$, $NH_4^+{}_{tot}$, N_2O, and NO_3^- by diffusion reaction modeling. Net $^{15}NH_4^+$ production (i.e., DNRA activity) was located at 5 to 10 mm of depth in the sediment, whereas net N_2O production (i.e., denitrification activity) was located at 3.5 to 8 mm of depth (Fig. 4). The layer of NO_3^- consumption was located at 3.5 to 8 mm of depth, whereas the layer of $NH_4^+{}_{tot}$ production was located at 6.5 to 11 mm of depth (Fig. 4). Depth-integrated DNRA and denitrification activities were, on average, 2.2 and 78.9 μmol N m^{-2} h^{-1}, respectively, whereas the depth-integrated $NH_4^+{}_{tot}$ production and NO_3^- consumption rates were, on average, 11.4 and 71.4 μmol N m^{-2} h^{-1}, respectively (data not shown).

Concentration profiles in marine sediment. Intertidal sediment cores were overlain with aerated seawater amended with 50 μmol liter^{-1} $^{15}NO_3^-$. Figure 5 shows the average concentration profiles measured in three replicate sediment cores; microsensor and gel probe profile determinations were repeated twice at random positions within each sediment core. The $^{15}NH_4^+$ concentration increased from 1.1 to 6.3 μmol liter^{-1} from the sediment surface to the 3.7-mm depth (Fig. 5A). The $^{15}NH_4^+$ concentration decreased to 5.1 μmol liter^{-1} at the 6.4-mm depth, and from there it increased to 7.1 μmol liter^{-1} at the 8.1-mm depth (Fig. 5A). The average standard deviation for all depth intervals was 1.2 μmol liter^{-1} $^{15}NH_4^+$. The N_2O profiles measured in acetylene-amended sediment cores showed an average peak concentration of 50 μmol liter^{-1} at the 3-mm depth (Fig. 5B). The $NH_4^+{}_{tot}$ concentration (measured with conventional gel probes) increased from 39.6 μmol liter^{-1} at the 0.5-mm depth to 157.7 μmol liter^{-1} at the 9.5-mm depth (Fig. 5C). At the 3.7-mm depth, where the peak $^{15}NH_4^+$ concentration of 6.3 μmol liter^{-1} was measured, an $NH_4^+{}_{tot}$ concentration of 82.1 μmol liter^{-1} was measured. The O_2 concentration decreased from 203 μmol liter^{-1} in the overlying water to 0 μmol liter^{-1} at the 3.5-mm depth (Fig. 5D). The total sulfide concentration was near the detection limit of 1 μmol liter^{-1} of the H_2S microsensor in the overlying water and in the sediment (Fig. 5D).

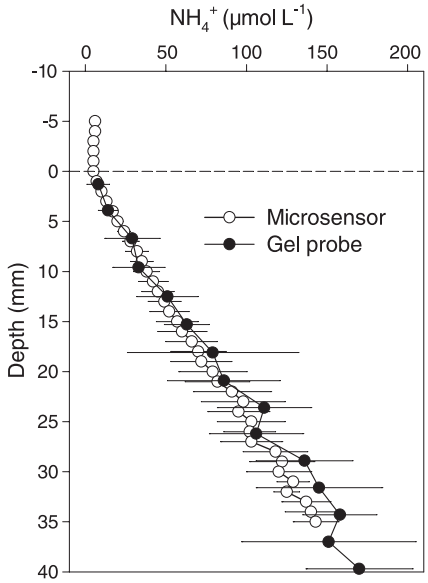

FIG. 2. Measurement of artificial $^{15}NH_4^+$ concentration gradients with the gel probe technique and microsensors. Quartz sand was incubated in benthic gradient chambers in which it was over- and underlain with potable water in which $^{15}NH_4^+$ concentration was continuously maintained at 0 and 250 μmol liter^{-1}, respectively. Thereby, a concentration gradient of $^{15}NH_4^+$ established in the pore water of the quartz sand. The means ± standard deviations of three to four replicate incubations are shown. The dashed line indicates the surface of the quartz sand layer.

Local conversion rates of $^{15}NH_4^+$, N_2O, and $NH_4^+{}_{tot}$ in marine sediment. Net $^{15}NH_4^+$ production (i.e., DNRA activity) was located at 3 to 6 mm of depth in the sediment, whereas net N_2O production (i.e., denitrification activity) was located at 0.75 to 4.5 mm of depth (Fig. 6). $NH_4^+{}_{tot}$ production was evident at 4 to 7 mm of depth (Fig. 6). The layer of NO_3^- consumption could not be located because NO_3^- measurements with conventional gel probes failed. The depth-integrated DNRA and denitrification activities were 2.1 and 61.4 μmol N m^{-2} h^{-1}, respectively, whereas the depth-integrated $NH_4^+{}_{tot}$ production rate was 13.7 μmol N m^{-2} h^{-1} (data not shown).

TABLE 2. Effect of He flushing on recovery of $^{15}NH_4^+$[a]

Duration of He flushing (min)	HCl concn (mol liter^{-1})	% $^{15}NH_4^+$ recovery	R^2 of regression line
2× 1	0	94	0.938
2× 1	1	111	0.955
1× 20	0	57	0.866
1× 20	1	79	0.968

[a] $^{15}NH_4^+$ recovery was calculated as the percentage of $^{15}NH_4^+$ retrieved by mass spectrometry from the nominal $^{15}NH_4^+$ concentration in the gel slices. Here, the average $^{15}NH_4^+$ recovery is given for the $^{15}NH_4^+$ concentrations 5, 10, and 25 μmol liter^{-1}, with five replicates each. $^{15}NH_4^+$ recoveries greater than 100% are explained by the low precision of the technique in the lower concentration range (Table 1).

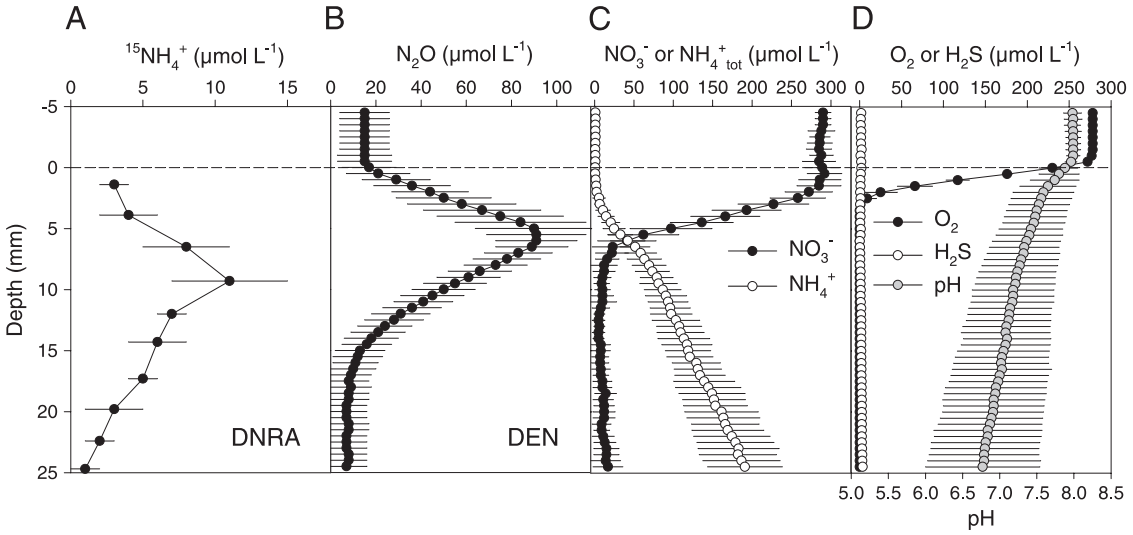

FIG. 3. Vertical profiles of $^{15}NH_4^+$ (A), N_2O (B), NO_3^- and $NH_4^+_{tot}$ (C), and O_2, H_2S, and pH (D) in freshwater sediment incubated in benthic gradient chambers. The $^{15}NH_4^+$ profiles (indicating DNRA activity) were measured with gel probes, while the remaining profiles were measured with microsensors. The N_2O profiles (indicating denitrification activity [DEN]) were measured upon inhibition of the last step of denitrification with acetylene. The means ± standard deviations of 6 to 15 replicate profiles in at least three replicate sediment samples are shown.

DISCUSSION

Assessment of the new technique. The combined gel probe and isotope labeling technique had a high precision over the concentration range of 0 to 25 µmol liter^{-1} $^{15}NH_4^+$. This range covered all concentrations in freshwater and marine sediments measured in this study. The absolute precisions were very similar for the calibration standards and sediment samples, with typical standard deviations being 1 to 2 µmol liter^{-1} $^{15}NH_4^+$. At a nominal $^{15}NH_4^+$ concentration of 0 µmol liter^{-1} in the calibration standards, the average standard deviation was 1.1 µmol liter^{-1}. Thus, the detection limit of the technique, defined as 3 times the standard deviation of the blank, was 3.3 µmol liter^{-1} $^{15}NH_4^+$. Exceptionally high standard deviations (and coefficients of variation) were measured in quartz sand with artificial $^{15}NH_4^+$ gradients that reached concentrations of up to 175 µmol liter^{-1}. However, the microsensor profiles measured in quartz sand also revealed high degrees of variability, especially in the high concentration range. It can therefore still be expected that the new gel probe technique is suitable for the precise measurement of $^{15}NH_4^+$ concentrations considerably higher than those in the sediments used in this study. One significant source of imprecision might be the water film on the gel surface that originates from the contact of the gel with the water column during retrieval of the probe. It is recommended either that the gel be carefully blotted dry before it is sliced or that cellulose acetate filter membranes that cover the gel during exposure and retrieval of the probe be used (25).

The accuracy of the new gel probe technique was calculated as the average deviation of the $^{15}NH_4^+$ concentrations (gel probe) from the $NH_4^+_{tot}$ concentrations (microsensors) measured in quartz sand with artificial $^{15}NH_4^+$ gradients. The absolute and relative accuracies of the gel probe technique were, on average, 0.6 µmol liter^{-1} $^{15}NH_4^+$ and 1.6%, respectively. However, this apparently high level of accuracy resulted

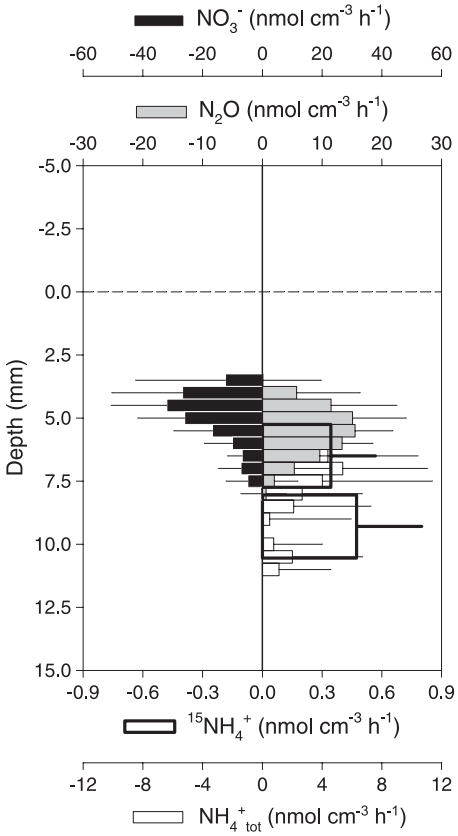

FIG. 4. Net rates of $^{15}NH_4^+$ production (i.e., DNRA), N_2O production (i.e., denitrification), $NH_4^+_{tot}$ production, and NO_3^- consumption in freshwater sediment. The rates were calculated from the concentration profiles in Fig. 3. For clarity, the rates of $^{15}NH_4^+$, N_2O, and $NH_4^+_{tot}$ consumption and the rates of NO_3^- production are not shown. The mean rates ± standard deviations are shown for each depth layer. Note the different scales.

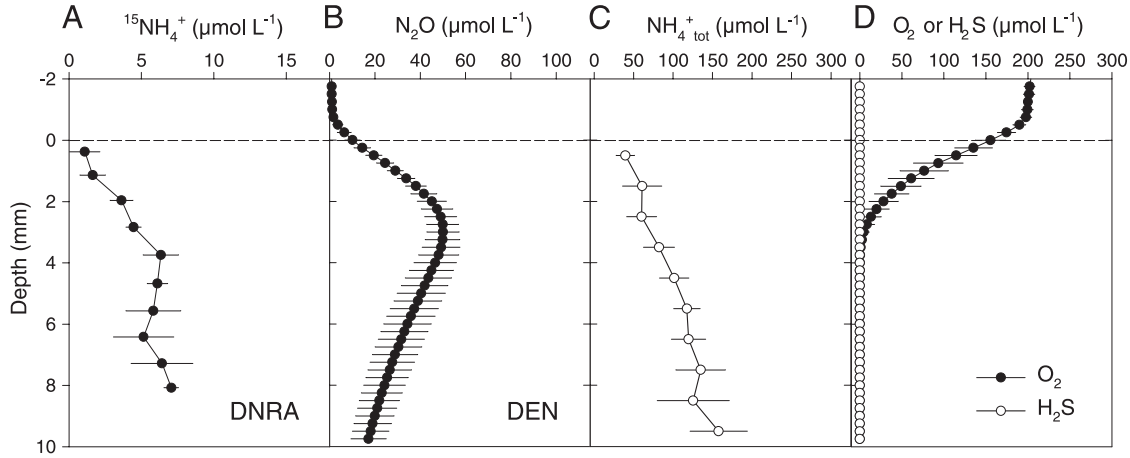

FIG. 5. Vertical profiles of $^{15}NH_4^+$ (A), N_2O (B), $NH_4^+{}_{tot}$ (C), and O_2 and H_2S (D) in intact cores of marine sediment. The means ± standard deviations of six profiles in three replicate sediment samples are shown. Other details are as described in the legend to Fig. 3.

from positive and negative deviations between the gel probe and the microsensor data that cancelled out each other. The stochastic nature of these deviations indicate, however, that there was no systematic under- or overestimation of the $^{15}NH_4^+$ concentration by the gel probe technique.

Calibrations of the gel probe technique were made either in quartz sand that was mixed with potable water or directly in potable water adjusted to contain different $^{15}NH_4^+$ concentrations. These two ways to calibrate the gel probes gave highly similar results in terms of accuracy (i.e., deviation from nominal concentrations), linearity, and scatter. It is thus recommended, for the ease of handling, that gel probes be calibrated for measurement of $^{15}NH_4^+$ concentrations in freshwater or seawater rather than in quartz sand. Calibrations in quartz sand should, however, be preferred whenever the time needed for diffusive equilibration in a porous medium is to be determined (e.g., when different gel types are tested).

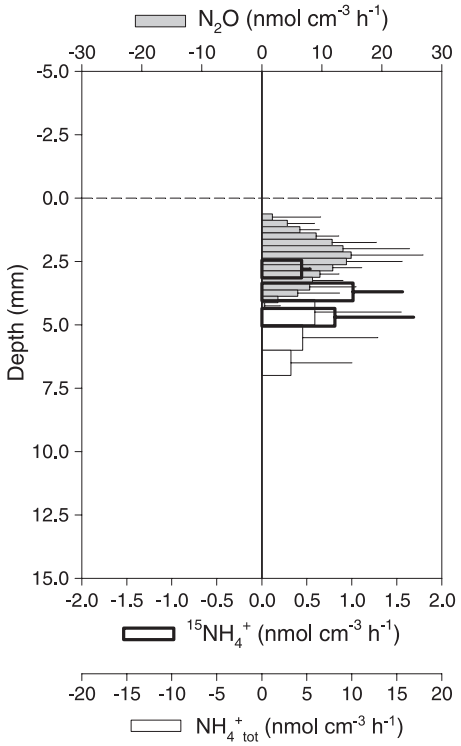

FIG. 6. Net rates of local $^{15}NH_4^+$ production (i.e., DNRA), N_2O production (i.e., denitrification), and $NH_4^+{}_{tot}$ production in marine sediment. The rates were calculated from the concentration profiles in Fig. 5. Other details are as described in the legend to Fig. 4. Note the different scales.

The recovery of $^{15}NH_4^+$ by the gel probe technique can be increased by acidification of the reaction assay mixtures before the reaction vials are flushed with He. While a thorough He flushing is necessary for the complete removal of ^{15}N-labeled N_2 from the reaction vials, especially when the gel probes are used in biological samples, it also leads to the loss of $^{15}NH_4^+$ in the form of $^{15}NH_3$. The results show that the loss of $^{15}NH_4^+$ is minimized by acidification of the reaction assay mixture. In theory, this measure might also hydrolyze organic compounds into which ^{15}N has been incorporated, thus giving a false-positive result due to $^{15}NH_3$ production. Therefore, it is recommended that this step be kept short and that the reaction vials be flushed with He for 2× 1 min (with a 5-min equilibration time between each flushing). It needs to be noted, however, that NaOH may also hydrolyze organic compounds that contain ^{15}N and that hypobromite itself may oxidize the ^{15}N in methylamines (46). False-positive results due to the use of NaOH and hypobromite might be avoided by quantifying $^{15}NH_4^+$ by chromatographic analysis (15).

Rapid slicing of the retrieved gels is essential to keep the vertical concentration gradients in the gel in shape. Long handling times will inevitably lead to the relaxation of gradients within the gel (10). The egg cutter principle proved to be most efficient to achieve rapid slicing. The total time that elapsed from retrieving the probe to cutting the gel was 60 s. Modeling the lateral diffusion within the gel revealed that during this handling time a 1-mm-wide, rectangular concentration peak would shrink by 15% in height and would approximately double in width (10). The layer of NO_3^- consumption in aquatic sediments usually spans several millimeters (32, 53), and it can be expected that the concentration peaks of NH_4^+ and N_2 are

also normally wider than 1 mm. Relaxation of such peaks will therefore be less pronounced than in the modeling example described above. The evenly spaced steel chords or blades of the egg cutters produce slices of similar size that allow a rough reconstruction of the vertical concentration profile. However, weighing of 100 gel slices revealed a coefficient of variation as high as 15%. Thus, weighing is recommended to improve the spatial accuracy of the reconstructed concentration profiles (34).

Comparison to other techniques. Conventional methods to investigate the relative importance of different pathways of dissimilatory NO_3^- reduction in sediments include slurry incubations (4, 12, 30), methods that use sealed sediment cores (7, 47), and methods that use flowthrough sediment cores (16, 27, 37). Only one study used reconstituted sediment cores in which DNRA activity was measured at centimeter-level resolution (39). Slurry incubations destroy the vertical gradients of pore water solutes, and every sediment particle and its attached bacteria are exposed to identical chemical conditions. Slurry incubations are run in batch mode and thus require high starting concentrations of NO_3^- that often exceed the *in situ* pore water concentrations of NO_3^- (4). Consequently, slurry incubations produce potential rather than actual rates (53). An exception to this observation is slurry incubations of permeable sands, which result in rates not higher than the actual rates measured in intact sediment cores (14). A clear advantage of slurry incubations is that they are suitable for use in manipulation experiments (6, 30).

Flux measurements using intact cores quantify the net solute exchange across the sediment-water interface due to microbial activities inside the sediment. Flux measurements are run in either batch mode (sealed cores) or continuous mode (flowthrough cores). Sealed cores face the same problem as slurry incubations because of high starting NO_3^- concentrations (47). Due to the batch mode, the ratio of electron acceptor (added to the water column as NO_3^-) to electron donor (present in the sediment as labile organic carbon or sulfide) changes during the experiment. The use of flowthrough cores solves this problem by maintaining a constant NO_3^- concentration in the water column throughout the experiment. As a consequence, steady-state fluxes of NO_3^-, NH_4^+, and N_2 across the sediment-water interface can be measured. For both types of flux measurements, however, the microenvironmental conditions in the sediment remain unknown.

Measurements in sediments. The combined gel probe and isotope labeling technique proved to be applicable in freshwater and marine sediments as well as in sterile quartz sand. The overall procedure of the gel probe technique was identical for these three types of samples, and only the salt concentration in each type of sample was adjusted during prehydration of the gel. Both the freshwater and the marine sediments exhibited a layer of net $^{15}NH_4^+$ production that in the case of the freshwater sediment overlapped the layer of net NO_3^- consumption in the anoxic part of the sediment. It is thus very likely that the $^{15}NH_4^+$ peak concentrations mainly resulted from DNRA activity. In contrast, the low $^{15}NH_4^+$ concentrations measured above and below the layer of dissimilatory NO_3^- may originate from the ^{15}N assimilated by bacteria during the incubation with $^{15}NO_3^-$. Future studies will verify this interpretation by the parallel analysis of functional genes indicative of DNRA (e.g., that for the cytochrome *c* nitrite reductase, *nrfA* [33]) in different sediment layers.

The relative fractions of $^{15}NH_4^+$ from $NH_4^+{}_{tot}$ in the layer of DNRA activity were only 13.6 and 7.7% in the freshwater and marine sediments, respectively. This means that most of the pore water NH_4^+ originated from processes other than DNRA, such as cell lysis and degradation of particulate organic matter. It is one of the strengths of the gel probe technique that it specifically quantifies NH_4^+ production by DNRA in the presence of other significant sources of NH_4^+ in the sediment. In contrast, sedimentary sinks of NH_4^+ will lead to an underestimation of the actual DNRA activity. Assimilation of NH_4^+, anaerobic oxidation of NH_4^+ (anammox), and adsorption of NH_4^+ to mineral surfaces should ideally be quantified together with DNRA to judge the degree of its underestimation by the gel probe technique. For instance, in the marine sediment, 10% of the experimentally added NH_4^+ (50 μmol liter^{-1}) adsorbed to mineral surfaces, while 90% was dissolved in the pore water (data not shown). Hence, 10% of the $^{15}NH_4^+$ produced by DNRA was possibly overlooked by the gel probe technique. A methodical underestimation of DNRA may also result from nitrification activity at the sediment surface, which dilutes the $^{15}NO_3^-$ pool with $^{14}NO_3^-$. In fact, the relative labeling level of NO_3^- (and thus nitrification activity) in different sediment depths could also be analyzed with the gel probe technique combined with determination of the level of bacterial conversion of NO_3^- to N_2 (45). In general, however, it should be kept in mind that the conversion rates measured with the gel probe technique, just like those measured with microsensors, represent net rather than gross conversion rates.

Acetylene-amended sediments exhibited a large N_2O concentration peak that for the freshwater sediment overlapped the layer of NO_3^- consumption in the anoxic part of the sediment. Such peaks are commonly ascribed to denitrification activity (44). In fact, the accumulation of N_2O in acetylene-amended sediments originates only from the denitrification driven by NO_3^- from the overlying water, while coupled nitrification-denitrification is inhibited (49). The method should therefore be used only with sediments overlain by a NO_3^--rich water column, which was the case for both the freshwater and the marine sediments studied here. The N_2O and $^{15}NH_4^+$ concentration peaks overlapped only partially and suggested that DNRA activity was located slightly deeper in the sediment than denitrification activity. This could be explained by the lower ratio of electron acceptor to electron donor in the layer of DNRA activity, which is commonly assumed to favor DNRA over denitrification (17, 55). One of the strengths of the new gel probe technique is that it localizes the layer of DNRA activity and thereby places it in a microenvironmental context that can be characterized with microsensors. The present study presents a first example of DNRA activity being associated with the low end of the NO_3^- gradient and denitrification activity being associated with somewhat higher NO_3^- concentrations. DNRA activity made up only 2.7 and 3.3% of the total dissimilatory NO_3^- reduction in the freshwater and marine sediments, respectively, which might be explained by the relatively low contents of particulate organic matter and sulfide in both sediments (48). It will therefore be interesting to analyze organic-rich sediments or sediments in which the

layer of NO_3^- consumption is intersected by a sulfide gradient from below. Sulfide can stimulate dissimilatory NO_3^- reduction by serving as an electron donor, especially in the water column (20, 28), but can also inhibit denitrification when it is present at high concentrations in the sediment (4). Presumably, in sulfidic sediments overlain by NO_3^--polluted water (8, 36), DNRA activity will make up a higher fraction of the total dissimilatory NO_3^- reduction and will be located slightly deeper in the sediment than denitrification activity.

ACKNOWLEDGMENTS

We are grateful to G. Eickert and I. Schröder for construction of the microsensors and to A. T. Schramm for NO_3^- and NH_4^+ analyses.

This study was financed by funds of the German Science Foundation granted to P.S. (STI202/4) and the Max Planck Society.

REFERENCES

1. **Andersen, K., T. Kjaer, and N. P. Revsbech.** 2001. An oxygen insensitive microsensor for nitrous oxide. Sensor. Actuat. B Chem. **81:**42–48.
2. **Boudreau, B. P.** 1996. The diffusive tortuosity of fine-grained unlithified sediments. Geochim. Cosmochim. Acta **60:**3139–3142.
3. **Broecker, W. S., and T.-H. Peng.** 1974. Gas exchange rates between air and sea. Tellus **26:**21–35.
4. **Brunet, R. C., and L. J. Garcia-Gil.** 1996. Sulfide-induced dissimilatory nitrate reduction to ammonia in anaerobic freshwater sediments. FEMS Microbiol. Ecol. **21:**121–130.
5. **Burgin, A. J., and S. K. Hamilton.** 2007. Have we overemphasized the role of denitrification in aquatic ecosystems? A review of nitrate removal pathways. Front. Ecol. Environ. **5:**89–96.
6. **Carini, S. A., B. N. Orcutt, and S. B. Joye.** 2003. Interactions between methane oxidation and nitrification in coastal sediments. Geomicrobiol. J. **20:**355–374.
7. **Christensen, P. B., R. N. Glud, T. Dalsgaard, and P. Gillespie.** 2003. Impacts of longline mussel farming on oxygen and nitrogen dynamics and biological communities of coastal sediments. Aquaculture **218:**567–588.
8. **Christensen, P. B., S. Rysgaard, N. P. Sloth, T. Dalsgaard, and S. Schwaerter.** 2000. Sediment mineralization, nutrient fluxes, denitrification and dissimilatory nitrate reduction to ammonium in an estuarine fjord with sea cage trout farms. Aquat. Microb. Ecol. **21:**73–84.
9. **Davison, W., and H. Zhang.** 1994. In-situ speciation measurements of trace components in natural waters using thin-film gels. Nature **367:**546–548.
10. **Davison, W., H. Zhang, and G. W. Grime.** 1994. Performance characteristics of gel probes for measuring the chemistry of pore waters. Environ. Sci. Technol. **28:**1623–1632.
11. **De Beer, D., A. Schramm, C. M. Santegoeds, and M. Kühl.** 1997. A nitrite microsensor for profiling environmental biofilms. Appl. Environ. Microbiol. **63:**973–977.
12. **Dong, L. F., C. J. Smith, S. Papaspyrou, A. Stott, A. M. Osborn, and D. B. Nedwell.** 2009. Changes in benthic denitrification, nitrate ammonification, and anammox process rates and nitrate and nitrite reductase gene abundances along an estuarine nutrient gradient (the Colne estuary, United Kingdom). Appl. Environ. Microbiol. **75:**3171–3179.
13. **Engström, P., T. Dalsgaard, S. Hulth, and R. C. Aller.** 2005. Anaerobic ammonium oxidation by nitrite (anammox): implications for N_2 production in coastal marine sediments. Geochim. Cosmochim. Acta **69:**2057–2065.
14. **Gao, H., F. Schreiber, G. Collins, M. M. Jensen, J. E. Kostka, G. Lavik, D. De Beer, H. Y. Zhou, and M. M. M. Kuypers.** 2010. Aerobic denitrification in permeable Wadden Sea sediments. ISME J. **4:**417–426.
15. **Gardner, W. S., H. A. Bootsma, C. Evans, and P. A. S. John.** 1995. Improved chromatographic analysis of $^{15}N/^{14}N$ ratios in ammonium or nitrate for isotope addition experiments. Mar. Chem. **48:**271–282.
16. **Gardner, W. S., and M. J. McCarthy.** 2009. Nitrogen dynamics at the sediment-water interface in shallow, sub-tropical Florida Bay: why denitrification efficiency may decrease with increased eutrophication. Biogeochemistry **95:**185–198.
17. **Gardner, W. S., M. J. McCarthy, S. An, D. Sobolev, K. S. Sell, and D. Brock.** 2006. Nitrogen fixation and dissimilatory nitrate reduction to ammonium (DNRA) support nitrogen dynamics in Texas estuaries. Limnol. Oceanogr. **51:**558–568.
18. **Glud, R. N., B. Thamdrup, H. Stahl, F. Wenzhoefer, A. Glud, H. Nomaki, K. Oguri, N. P. Revsbech, and H. Kitazato.** 2009. Nitrogen cycling in a deep ocean margin sediment (Sagami Bay, Japan). Limnol. Oceanogr. **54:**723–734.
19. **Gruber, N., and J. N. Galloway.** 2008. An Earth-system perspective of the global nitrogen cycle. Nature **451:**293–296.
20. **Hannig, M., G. Lavik, M. M. M. Kuypers, D. Woebken, W. Martens-Habbena, and K. Jurgens.** 2007. Shift from denitrification to anammox after inflow events in the central Baltic Sea. Limnol. Oceanogr. **52:**1336–1345.
21. **Herbert, R. A.** 1999. Nitrogen cycling in coastal marine ecosystems. FEMS Microbiol. Rev. **23:**563–590.
22. **Jeroschewski, P., C. Steuckart, and M. Kühl.** 1996. An amperometric microsensor for the determination of H_2S in aquatic environments. Anal. Chem. **68:**4351–4357.
23. **Kelly-Gerreyn, B. A., M. Trimmer, and D. J. Hydes.** 2001. A diagenetic model discriminating denitrification and dissimilatory nitrate reduction to ammonium in a temperate estuarine sediment. Mar. Ecol. Prog. Ser. **220:**33–46.
24. **Kempers, A. J., and C. J. Kok.** 1989. Re-examination of the determination of ammonium as the indophenol blue complex using salicylate. Anal. Chim. Acta **221:**147–155.
25. **Krom, M. D., P. Davison, H. Zhang, and W. Davison.** 1994. High-resolution pore-water sampling with a gel sampler. Limnol. Oceanogr. **39:**1967–1972.
26. **Kühl, M.** 2005. Optical microsensors for analysis of microbial communities. Environ. Microbiol. **397:**166–199.
27. **Laverman, A. M., C. Meile, P. Van Cappellen, and E. B. A. Wieringa.** 2007. Vertical distribution of denitrification in an estuarine sediment: integrating sediment flowthrough reactor experiments and microprofiling via reactive transport modeling. Appl. Environ. Microbiol. **73:**40–47.
28. **Lavik, G., T. Stührmann, V. Brüchert, A. Van der Plas, V. Mohrholz, P. Lam, M. Mußmann, B. M. Fuchs, R. Amann, U. Lass, and M. M. M. Kuypers.** 2008. Detoxification of sulphidic African shelf waters by blooming chemolithotrophs. Nature **457:**581–584.
29. **Li, Y. H., and S. Gregory.** 1974. Diffusion of ions in sea water and in deep-sea sediments. Geochim. Cosmochim. Acta **38:**703–714.
30. **Magalhaes, C. M., S. B. Joye, R. M. Moreira, W. J. Wiebe, and A. A. Bordalo.** 2005. Effect of salinity and inorganic nitrogen concentrations on nitrification and denitrification rates in intertidal sediments and rocky biofilms of the Douro River estuary, Portugal. Water Res. **39:**1783–1794.
31. **Martinez-Garcia, M., P. Stief, M. Diaz-Valdes, G. Wanner, A. Ramos-Espla, N. Dubilier, and J. Anton.** 2008. Ammonia-oxidizing Crenarchaeota and nitrification inside the tissue of a colonial ascidian. Environ. Microbiol. **10:**2991–3001.
32. **Meyer, R. L., T. Kjaer, and N. P. Revsbech.** 2001. Use of NO_x– microsensors to estimate the activity of sediment nitrification and NO_x– consumption along an estuarine salinity, nitrate, and light gradient. Aquat. Microb. Ecol. **26:**181–193.
33. **Mohan, S. B., M. Schmid, M. Jetten, and J. Cole.** 2004. Detection and widespread distribution of the *nrfA* gene encoding nitrite reduction to ammonia, a short circuit in the biological nitrogen cycle that competes with denitrification. FEMS Microbiol. Ecol. **49:**433–443.
34. **Mortimer, R. J. G., M. D. Krom, P. O. J. Hall, S. Hulth, and S. Stahl.** 1998. Use of gel probes for the determination of high resolution solute distributions in marine and estuarine pore waters. Mar. Chem. **63:**119–129.
35. **Nielsen, L. P.** 1992. Denitrification in sediment determined from nitrogen isotope pairing. FEMS Microbiol. Ecol. **86:**357–362.
36. **Nizzoli, D., D. T. Welsh, E. A. Fano, and P. Viaroli.** 2006. Impact of clam and mussel farming on benthic metabolism and nitrogen cycling, with emphasis on nitrate reduction pathways. Mar. Ecol. Prog. Ser. **315:**151–165.
37. **Porubsky, W. P., L. E. Velasquez, and S. B. Joye.** 2008. Nutrient-replete benthic microalgae as a source of dissolved organic carbon to coastal waters. Estuar. Coast. **31:**860–876.
38. **Porubsky, W. P., N. B. Weston, and S. B. Joye.** 2009. Benthic metabolism and the fate of dissolved inorganic nitrogen in intertidal sediments. Estuar. Coast. Shelf Sci. **83:**392–402.
39. **Preisler, A., D. De Beer, A. Lichtschlag, G. Lavik, A. Boetius, and B. B. Jørgensen.** 2007. Biological and chemical sulfide oxidation in a *Beggiatoa* inhabited marine sediment. ISME J. **1:**341–353.
40. **Pringault, O., R. de Wit, and P. Caumette.** 1996. A benthic gradient chamber for culturing phototrophic sulfur bacteria on reconstituted sediments. FEMS Microbiol. Ecol. **20:**237–250.
41. **Revsbech, N. P.** 1989. An oxygen microsensor with a guard cathode. Limnol. Oceanogr. **34:**474–478.
42. **Revsbech, N. P.** 2005. Analysis of microbial communities with electrochemical microsensors and microscale biosensors. Methods Enzymol. **397:**147–166.
43. **Revsbech, N. P., B. B. Jørgensen, T. H. Blackburn, and Y. Cohen.** 1983. Microelectrode studies of the photosynthesis and O_2, H_2S, and pH profiles of a microbial mat. Limnol. Oceanogr. **28:**1062–1074.
44. **Revsbech, N. P., L. P. Nielsen, P. B. Christensen, and J. Sørensen.** 1988. Combined oxygen and nitrous oxide microsensor for denitrification studies. Appl. Environ. Microbiol. **54:**2245–2249.
45. **Risgaard-Petersen, N., S. Rysgaard, and N. P. Revsbech.** 1993. A sensitive assay for determination of $^{14}N/^{15}N$ isotope distribution in NO_3^-. J. Microbiol. Methods **17:**155–164.
46. **Risgaard-Petersen, N., S. Rysgaard, and N. P. Revsbech.** 1995. Combined microdiffusion-hypobromite oxidation method for determining ^{15}N isotope in ammonium. Soil Sci. Soc. Am. J. **59:**1077–1080.
47. **Rysgaard, S., R. N. Glud, N. Risgaard-Petersen, and T. Dalsgaard.** 2004. Denitrification and anammox activity in Arctic marine sediments. Limnol. Oceanogr. **49:**1493–1502.

48. **Scott, J. T., M. J. McCarthy, W. S. Gardner, and R. D. Doyle.** 2008. Denitrification, dissimilatory nitrate reduction to ammonium, and nitrogen fixation along a nitrate concentration gradient in a created freshwater wetland. Biogeochemistry **87:**99–111.
49. **Seitzinger, S. P., L. P. Nielsen, J. Caffrey, and P. B. Christensen.** 1993. Denitrification measurements in aquatic sediments: a comparison of three methods. Biogeochemistry **23:**147–167.
50. **Sloth, N. P., L. P. Nielsen, and T. H. Blackburn.** 1992. Nitrification in sediment cores measured with acetylene inhibition. Limnol. Oceanogr. **37:** 1108–1112.
51. **Sørensen, J.** 1978. Denitrification rates in a marine sediment as measured by the acetylene inhibition technique. Appl. Environ. Microbiol. **36:**139–143.
52. **Stief, P., and D. De Beer.** 2002. Bioturbation effects of *Chironomus riparius* on the benthic N-cycle as measured using microsensors and microbiological assays. Aquat. Microb. Ecol. **27:**175–185.
53. **Stief, P., and D. De Beer.** 2006. Probing the microenvironment of freshwater sediment macrofauna: implications of deposit-feeding and bioirrigation for nitrogen cycling. Limnol. Oceanogr. **51:**2538–2548.
54. **Stockdale, A., W. Davison, and H. Zhang.** 2009. Micro-scale biogeochemical heterogeneity in sediments: a review of available technology and observed evidence. Earth-Sci. Rev. **92:**81–97.
55. **Tiedje, J. M., A. J. Sexstone, D. D. Myrold, and J. A. Robinson.** 1982. Denitrification: ecological niches, competition and survival. Antonie Van Leeuwenhoek **48:**569–583.
56. **Warembourg, F. R.** 1993. Nitrogen fixation in soil and plant systems, p. 157–180. *In* R. Knowles and T. H. Blackburn (ed.), Nitrogen isotope techniques. Academic Press, New York, NY.